Hepat Mon. 2026; 26(1): e171094 https://doi.org/10.5812/hepatmon-171094

Published Online: 2026 May 20 **Research Article**

Longitudinal Serum Proteomic and Metabolomic Profiling of Chronic Hepatitis B During Tenofovir Disoproxil Fumarate Therapy

Peixia Lin [#1], Zhaojun Jin [#1], Yimin Chen [1], Jiaxin Jin [1], Min Deng [2,*], Dahai Wei [3,**]

[1] Zhejiang Chinese Medical University, Hang-zhou, China
[2] Department of Infectious Diseases, Affiliated Hospital of Jiaxing University, Jiaxing, China
[3] Institute of Liver Diseases, Affiliated Hospital of Jiaxing University, Jiaxing, China

[*] ***Corresponding Author:*** Department of Infectious Diseases, Affiliated Hospital of Jiaxing University, Jiaxing, China. Email: milixiaozhu@163.com
[**] ***Corresponding Author:*** Institute of Liver Diseases, Affiliated Hospital of Jiaxing University, Jiaxing, China. Email: weidahai3166@hotmail.com
# These authors have contributed equally

Received: 20 March, 2026; **Revised:** 20 April, 2026; **Accepted:** 29 April, 2026

Abstract

Background: Hepatitis B virus (HBV) infection remains a major global health burden. Although tenofovir disoproxil fumarate (TDF) effectively suppresses HBV replication, its precise mechanism of action remains incompletely understood.

Objectives: This exploratory study aimed to track longitudinal serum proteomic and metabolomic alterations associated with effective TDF therapy in patients with chronic hepatitis B (CHB) and to elucidate their potential roles in mediating physiological processes and disease progression across different stages of therapy.

Methods: Using data-independent acquisition (DIA) proteomics and untargeted metabolomics with ultra-high-performance liquid chromatography-quadrupole-Orbitrap tandem mass spectrometry (UHPLC-Q-Orbitrap MS/MS), we analyzed serum protein and metabolite profiles from 18 patients with CHB receiving TDF therapy. Samples were collected before treatment initiation (baseline, CO) and at weeks 12 (TDF-12) and 24 (TDF-24) of therapy.

Results: Proteomic analysis identified 83 and 104 differentially expressed proteins at TDF-12 and TDF-24, respectively. Metabolomic profiling revealed 101 and 105 significantly altered metabolites at the same time points. Notably, at the predefined treatment response endpoint (week 24; HBV DNA < 30 IU/mL), integrated pathway analysis showed the greatest enrichment in the peroxisome proliferator-activated receptor (PPAR) signaling pathway. Key molecules, including fatty acid-binding protein 5 (FABP5), apolipoprotein A-V (APOA5), 3-hydroxybutyric acid (BHB), and leukotriene B4 (LTB4), were identified as candidate biomarkers warranting further investigation.

Conclusions: To our knowledge, this is the first study to use an integrated, untargeted metabolomic and proteomic approach to characterize alterations in metabolites and proteins across different stages of TDF treatment in patients with CHB. These findings may provide a foundation for generating new hypotheses regarding the molecular mechanisms underlying the therapeutic response to TDF.

Keywords: Chronic Hepatitis B, Tenofovir Disoproxil Fumarate, Serum Metabolomics And Proteomics, PPAR Signaling Pathway

1. Background

Hepatitis B virus (HBV) infection remains a major public health concern worldwide, despite the availability of effective vaccines and antiviral therapies (1, 2). According to a recent systematic review incorporating World Health Organization (WHO) reports, an estimated 1.2 million new HBV infections occurred globally in 2022, with approximately 250 million people living with chronic HBV infection (3). Active viral replication causes necroinflammatory liver injury and related complications, including liver cirrhosis and hepatocellular carcinoma (HCC), resulting in approximately 1.13 million deaths annually (4, 5). Over the past few decades, clinical and basic research has substantially advanced our understanding of HBV characteristics, its natural history, and the immunopathogenesis of chronic hepatitis B (CHB) (2, 3).

How to Cite: Lin P, Jin Z, Chen Y, Jin J, Deng M, et al. Longitudinal Serum Proteomic and Metabolomic Profiling of Chronic Hepatitis B During Tenofovir Disoproxil Fumarate Therapy. Hepat Mon. 2026;26(1):e171094. doi: https://doi.org/10.5812/hepatmon-171094

The widespread use of antiviral therapies has significantly reduced the incidence of new HBV infections and mortality from HBV-related complications (6). Currently, two primary treatment strategies are used to suppress HBV replication in patients with CHB, thereby preventing or delaying progression to advanced stages of liver disease: a short-term immunomodulatory approach using agents such as pegylated interferon alpha (Peg-IFN-α) and a long-term strategy based on nucleos(t)ide analogues (NAs), including adefovir dipivoxil (ADV), entecavir (ETV), tenofovir alafenamide fumarate (TAF), and tenofovir disoproxil fumarate (TDF) (6-8). Among these, TDF is one of the most widely used first-line NAs in clinical practice; it competitively binds to the active site of HBV DNA polymerase, thereby inhibiting viral reverse transcriptase activity and suppressing HBV replication (9-11).

As a nucleos(t)ide reverse transcriptase inhibitor (NRTI) prodrug, TDF is chemically modified with a disoproxil moiety, a key structural modification that substantially increases its oral bioavailability by overcoming the low gastrointestinal absorption of its parent compound, tenofovir (11). After oral administration, TDF is hydrolyzed to tenofovir, which is subsequently phosphorylated intracellularly to the active metabolite tenofovir diphosphate (TFV-DP) (12). By competitively inhibiting HBV reverse transcriptase, TFV-DP halts viral DNA chain elongation and reduces the formation of covalently closed circular DNA (cccDNA) (12, 13). Through this mechanism, TDF effectively lowers serum HBV DNA levels and exhibits antiviral activity against wild-type, precore mutant, and lamivudine-resistant HBV strains (11, 12). In two large phase III trials enrolling hepatitis B e antigen (HBeAg)-negative and HBeAg-positive patients, TDF 300 mg/day showed significantly greater efficacy than ADV 10 mg/day in achieving virological suppression and histological improvement at both 48 and 96 weeks of treatment (14). Further research indicates that patients receiving TDF have a significantly lower risk of HBV-related HCC than those treated with ETV, with this benefit particularly pronounced in HBeAg-positive patients (13, 15). This conclusion is supported by a systematic review of 90,897 treatment-naïve patients with CHB, which demonstrated a significantly lower cumulative incidence of HCC in the TDF group (hazard ratio, 0.66; 95% confidence interval [CI], 0.56 - 0.76) (16). Collectively, these studies demonstrate that TDF has potent antiviral activity, sustained HBV suppression, favorable tolerability, a substantial genetic barrier to resistance, and a significantly reduced risk of HBV-related disease, thereby increasing clinical interest in NA therapies (10, 11, 15). However, the precise mechanisms by which TDF mediates these therapeutic outcomes remain incompletely understood and warrant further investigation.

In chronic HBV infection, effective coordination between innate and adaptive immune mechanisms is critical for successful disease management. The innate immune response during early infection plays a pivotal role in initiating and shaping the adaptive immune response, ultimately determining viral clearance through the immune system's capacity to recognize and effectively target HBV (4, 9, 17). As previously reported, TDF modulates the host immune response in patients with CHB to promote viral control, an effect characterized by elevated interferon-lambda 3 (IFN-λ3) levels and mediated primarily through the downregulation of peripheral regulatory T cell (Treg) frequency, restoration of skewed T-cell receptor beta-chain (TRBV) repertoire diversity, and reductions in alanine aminotransferase (ALT) levels (15, 18). Furthermore, TDF alters the expression of interferon-inducible protein 10 (IP-10) and other cytokines, thereby shaping an immune microenvironment that favors HBV suppression (19). In our previous quantitative proteomics study, we found that proteins upregulated during combination therapy with TDF and Peg-IFN-α were predominantly enriched in biological processes including the pentose phosphate pathway, the relaxin signaling pathway, and the gonadotropin-releasing hormone signaling pathway, whereas downregulated proteins were mainly associated with cholesterol metabolism and the herpes simplex virus 1 infection pathway (9). These findings suggest that TDF enhances antiviral effects by strengthening immune function. The level of HBV suppression is a strong indicator of clinical recovery; however, the molecular processes underlying the antiviral activity of TDF remain incompletely understood.

In recent years, high-throughput detection technologies have enabled comprehensive profiling of protein and metabolite targets by simultaneously quantifying multiple analytes in blood samples, thereby facilitating studies of host-pathogen interactions during viral infections in humans, animals, and plants (20-24). These technologies not only facilitate early detection, diagnosis, and disease monitoring across diverse diseases but also comprehensively reveal alterations in host factors and signaling pathways associated with viral infection, thereby enhancing our understanding of the molecular mechanisms underlying pathogenesis (17, 18). Accordingly, serum proteomic and metabolomic analyses enable

comprehensive characterization of host factors implicated in HBV infection and delineation of signaling pathway alterations associated with diverse classes of proteins and metabolites. Nevertheless, longitudinal multi-omics profiling of serum proteomic and metabolomic changes in patients with CHB during TDF therapy has not yet been reported.

2. Objectives

This study primarily aimed to define the longitudinal proteomic and metabolomic signatures of CHB disease progression during TDF therapy. We aimed to identify stage-associated molecular signatures and enriched pathways that may serve as a foundation for generating hypotheses regarding treatment mechanisms and for future research into potential biomarkers to complement existing clinical monitoring. To achieve this, we used data-independent acquisition (DIA) coupled with liquid chromatography-tandem mass spectrometry (LC-MS/MS) for serum proteomic analysis, along with ultra-high-performance liquid chromatography-quadrupole-Orbitrap tandem mass spectrometry (UHPLC-Q-Orbitrap MS/MS) for serum metabolomic profiling, to track unbiased differentially expressed protein and metabolite profiles in patients with CHB during TDF therapy. Accordingly, the findings of this study enable the tracking of the molecular timeline of TDF therapy, provide deeper insights into its underlying mechanisms, and offer a reference for subsequent investigations.

3. Methods

3.1. Patients and Sample Selection

Longitudinal serum samples were obtained from treatment-naïve adults aged 18 - 65 years who were diagnosed with CHB at the Affiliated Hospital of Jiaxing University between December 2023 and October 2024. This retrospective observational study used archived serum samples from a dedicated clinical biobank of patients who received TDF monotherapy and underwent routine virological monitoring. Only samples with complete serial collections and fully annotated clinical data were selected. All selected samples had undergone prior quality assessment; accordingly, no samples were excluded at any stage because of quality control (QC) failure in subsequent omics analyses. Eligible patients met the diagnostic criteria established in the WHO 2024 HBV guidelines and received continuous TDF monotherapy for at least 48 weeks. The primary reference standard for evaluating treatment efficacy was a predefined effective virologic response, defined as achieving a serum HBV DNA level below 30 IU/mL at week 24 of treatment. In addition, response status at weeks 12 and 24 was evaluated based on the magnitude of the decrease in HBV DNA load relative to baseline. The following exclusion criteria were applied to all potential participants within the 12 months prior to enrollment: absolute contraindications to TDF, pregnancy, history of solid organ or bone marrow transplantation, coinfection with other viruses, autoimmune or immune-mediated disorders, clinically significant metabolic diseases, decompensated liver disease, clinically relevant neuropsychiatric disorders, primary HCC or other malignancies, or severe dysfunction of major organ systems. Before study initiation, the study was approved by the Ethics Committee of the Affiliated Hospital of Jiaxing University (No. 2023-LY-519), and written informed consent was obtained from all participants or their legal guardians. All procedures were conducted in accordance with the ethical standards of the Declaration of Helsinki.

For integrated proteomic and metabolomic profiling, serum samples were prospectively collected from 18 randomly selected patients with CHB who achieved an effective virologic response to TDF treatment. To evaluate molecular changes associated with treatment response, we defined a prespecified virologic response endpoint as an HBV DNA load below 30 IU/mL at week 24 of TDF therapy. Samples were collected at 3 time points: before treatment initiation (baseline, CO), at week 12 of TDF treatment (TDF-12), and at week 24 of TDF treatment (TDF-24). To ensure analytical rigor and mitigate technical bias, stringent QC measures were implemented throughout the experimental workflow. First, blinding was enforced: the laboratory analyst responsible for sample preparation, instrumental analysis, and preliminary data processing was unaware of the clinical groupings. Second, injection order was randomized: All serum samples were processed within a single analytical batch, and the injection sequence was randomized computationally to evenly distribute potential confounding factors. Third, systematic quality monitoring was conducted: a pooled QC sample generated from equal-pooled aliquots of all study samples was injected at the beginning of the analytical run and subsequently after every 8 to 10 experimental samples to continuously assess instrumental stability. Finally, data refinement and normalization were performed: metabolic or proteomic features with a relative standard deviation greater than 30% in QC replicates were considered unstable and removed. The stable feature set was then normalized using probabilistic quotient normalization, with the pooled QC sample serving as the reference to correct for

intra-batch signal drift. Because the entire sample set was analyzed in a single batch, inter-batch correction was unnecessary. The overall technical framework of this project is illustrated in Figure S1.

3.2. Protein Extraction and Trypsin Digestion for DIA LC-MS/MS-Based Serum Proteomic Analysis

After clarification at 12,000 × g for 10 min at 4 °C, the supernatant was transferred to a new tube, and low-abundance proteins were enriched using magnetic beads according to the manufacturer's guidelines. Briefly, 4 µL of prewashed magnetic beads were incubated with 100 µL of serum/plasma for 2 h on a magnetic rack, followed by five 5-min washes to remove unbound components. Before in-solution digestion, proteins on the beads were processed sequentially as follows: after lysis and denaturation in UA buffer, disulfide bonds were reduced with 20 mM dithiothreitol at 37 °C for 1 h with gentle shaking and subsequently alkylated with iodoacetamide for 30 min at room temperature in the dark. After dilution with 50 mM NH_4HCO_3 to a urea concentration < 1.5 M and centrifugation, the supernatant was digested with trypsin at a ratio of 1:50 w/w at 37 °C for 16 h. The digest was then desalted on a C18 column (Sigma, USA), dried under vacuum, and redissolved in 20 µL of 0.1% formic acid. Finally, peptide concentration was measured by UV spectrophotometry at 280 nm.

All data were acquired in DIA mode using a Thermo Fisher Orbitrap Astral mass spectrometer equipped with an Easy-Spray source and coupled online to a Vanquish Neo UHPLC system. For quantitative LC-MS/MS, peptides were separated on a 15-cm ES906 column at 800 nL/min using a binary gradient of 0.1% formic acid in water (A) and 80% acetonitrile/0.1% formic acid (B). Mass spectrometric data were acquired on an Orbitrap Astral in DIA mode. MS1 scans at 380 - 980 m/z were collected at a resolution of 240,000 at 200 m/z, with a 500% normalized automatic gain control target and a 5-ms maximum injection time. For MS2, 299 × 2 m/z isolation windows were used with higher-energy collisional dissociation at 25 eV, a 500% automatic gain control target, and a 3-ms maximum injection time. DIA-NN version 1.8.1 processing parameters included trypsin digestion with a maximum of 1 missed cleavage, static carbamidomethylation (C), variable oxidation (M), and N-terminal acetylation. Identifications were filtered at a 1% false discovery rate.

3.3. Extraction, Collection, and Preparation of Compounds for UHPLC-Q-Orbitrap MS/MS-Based Serum Metabolomics Analysis

Serum proteins were precipitated with cold methanol/acetonitrile (1:1, 4:1 v/v), followed by centrifugation at 15,000 × g for 20 min at 4 °C. The dried supernatant was reconstituted in acetonitrile/H_2O (1:1), centrifuged at 15,000 × g for 15 min at 4 °C to clarify, and the supernatant was analyzed by UHPLC-Q-Orbitrap MS/MS. Metabolomic profiling was conducted using a Thermo Vanquish UHPLC system coupled to an Orbitrap Exploris 480 mass spectrometer. Chromatographic separation was achieved on a Waters ACQUITY UPLC BEH Amide column (2.1 × 100 mm, 1.7 µm) under hydrophilic interaction liquid chromatography conditions. The mobile phase comprised 25 mM ammonium acetate/ammonium hydroxide in water and acetonitrile, with a gradient from 95% to 40% acetonitrile over 0 - 5.5 min, followed by re-equilibration for a total run time of 8 min. Data were acquired in both positive and negative electrospray ionization modes with the following source parameters: GS1, 50; GS2, 2; temperature, 350 °C; spray voltage, +3500 V in positive mode and -2800 V in negative mode. Full-scan MS data at m/z 70 - 1200 were collected at a resolution of 60,000 with a maximum injection time of 100 ms. For MS/MS, data-dependent acquisition was applied, with dynamic exclusion set to 4 s.

Raw UHPLC-MS data were processed as follows: conversion to mzXML using ProteoWizard MSConvert, followed by feature extraction in XCMS using the centWave algorithm with a peak width of 10 - 60 s, an m/z tolerance of 10 ppm, and a prefilter of 10 intensity and 100 peaks. Peak grouping parameters were bw = 5, mzwid = 0.025, and minfrac = 0.5. Features detected in < 50% of samples per group were removed. Metabolites were annotated by matching accurate mass within ± 10 ppm and MS/MS spectra against an in-house standard library. Following sum normalization, Pareto-scaled multivariate analysis, including principal component analysis (PCA) and orthogonal partial least-squares discriminant analysis (OPLS-DA), was performed using the ropls R package. The OPLS-DA model was validated by 7-fold cross-validation and permutation testing. Metabolites were then ranked based on their variable importance in projection scores derived from the OPLS-DA model.

3.4. Bioinformatics Analysis of the Differentially Expressed Proteins and Metabolites

Differentially expressed molecules, including proteins and metabolites, identified using statistical significance and fold-change thresholds, were subjected to hierarchical clustering analysis. Hierarchical clustering was performed using Euclidean distance and

average linkage with Cluster 3.0 software. The resulting dendrograms and heatmaps were visualized using Java TreeView. For functional annotation, homologous sequences were identified via local BLAST using NCBI BLAST+ version 2.2.28+. Gene Ontology (GO) annotation was performed with Blast2GO, assigning terms across the 3 GO categories. Protein and metabolite lists were mapped to the Kyoto Encyclopedia of Genes and Genomes (KEGG) database for pathway enrichment analysis using KEGG Orthology identifiers.

3.5. Integrated Correlation Analysis of Proteomic and Metabolomic Data

To investigate interrelationships between the proteome and metabolome, we first performed correlation analysis between the 2 datasets. Subsequently, to explore functional convergence, we conducted pathway-level integration analysis using the Joint Pathway Analysis module in MetaboAnalyst 6.0, which systematically examined relationships between dysregulated proteins and metabolites within biological pathways. Based on the KEGG database, these molecules were separately subjected to pathway annotation and enrichment analysis. The resulting omics datasets were then integrated using R software version 3.5.1 and visualized using Venn diagrams and bar plots to illustrate convergent and distinct pathway activities.

3.6. Validation of Selected Dysregulated Proteins and Metabolites

To further validate the proteomics and metabolomics results, serum samples from all 3 groups were evaluated using enzyme-linked immunosorbent assay (ELISA) and automated biochemical analysis, following standardized protocols as previously described, to screen for selected dysregulated proteins and metabolites (9, 25). Briefly, samples were thawed, centrifuged, and aliquoted before analysis using a commercial ELISA kit. Quantification of target proteins and metabolites was performed in triplicate on a BioTek ELX 800 microplate reader. Concentrations were automatically calculated against a standard curve with appropriate dilutions. To further validate the diagnostic potential of the identified proteins and metabolites, we performed receiver operating characteristic (ROC) analysis in MedCalc, comparing the area under the curve (AUC) and its 95% CI for statistical significance.

3.7. Statistical Analysis

Statistical analyses were performed in SPSS version 22.0 (SPSS Inc., Chicago, IL, USA). Data are reported as the mean ± SD or median (IQR) for continuous variables and as n (%) for categorical variables, based on normality testing. Between-group comparisons used the independent *t*-test, Mann-Whitney U test, or chi-square/Fisher exact test, as appropriate. A 2-tailed P value < 0.05 was considered statistically significant. Given the exploratory nature of this study, which aimed to generate hypotheses, no adjustment for multiple testing was applied. Therefore, all reported associations and candidate biomarkers should be interpreted as preliminary and require validation in future independent cohorts.

In the exploratory identification of differentially expressed proteins and metabolites, a threshold of unadjusted P value < 0.05 combined with a fold change ≥ 1.5 for upregulation or ≤ 0.67 for downregulation was applied to maximize sensitivity. For metabolites, significance in the OPLS-DA model, variable importance in projection > 1.0, and cross-validation were also considered. The identified candidate molecules are presented as preliminary findings for future validation.

4. Results

4.1. Clinical Characteristics of Participants

A total of 162 usable serum samples were successfully obtained and processed from 54 patients with CHB with sustained HBV DNA suppression < 30 IU/mL following TDF therapy, with 1 sample per patient at CO, TDF-12, and TDF-24. Notably, all planned samples from the 18-patient discovery cohort yielded valid proteomic and metabolomic data, forming a complete dataset with no missing samples or failed runs for subsequent analyses. These samples were stratified into 2 cohorts: a discovery cohort comprising 54 serum samples from 18 patients with CHB for comprehensive proteomic and metabolomic profiling based on treatment duration, and a validation cohort consisting of 108 serum samples from 36 patients with CHB for targeted validation of dysregulated proteins and metabolites identified in the discovery phase. Comparative analysis revealed that age, alkaline phosphatase (AKP), aspartate aminotransferase (AST), HBeAg status, and total bilirubin (TBIL) levels did not differ significantly across groups. However, hepatitis B surface antigen (HBsAg) and HBV DNA load differed significantly in the TDF-12 and TDF-24 groups compared with the CO group. Platelet counts differed significantly between the TDF-12 and CO groups. In addition, significant differences were observed between the TDF-24 and CO groups in ALT, glutamyl transpeptidase (GGT), and creatinine (Cr) (Table 1).

Table 1. Baseline Characteristics of Patients Enrolled in This Study

Clinical Indicators	CO group	TDF-12 group	TDF-24 group
Age (y)	41.67 ± 3.50	41.67 ± 3.50	41.67 ± 3.50
HBsAg (log_{10} IU/mL)	4.13 ± 0.62	2.85 ± 0.58 [a]	2.47 ± 0.63 [b]
HBeAg (%)	94	88	77
HBV DNA (log_{10}IU/mL)	6.18 ± 1.81	3.07 ± 0.78 [a]	< 1.48 [b]
ALT (IU/L)	56.1 ± 6.43	51.11 ± 10.98	36.33 ± 16.87 [b]
AST (IU/L)	53.56 ± 7.86	51.22 ± 6.40	46.89 ± 5.99
TBIL (μmol/L)	11.74 ± 2.42	11.82 ± 1.33	10.74 ± 2.01
GGT (IU/L)	57.22 ± 16.01	43.82 ± 14.78	43.99 ± 13.86 [b]
AKP (IU/L)	71.00 ± 6.26	81.67 ± 9.19	77.56 ± 7.72
Cr (ummol/L)	75.3 ± 4.99	73.09 ± 4.28	68.13 ± 4.72 [b]
PLT ($\times 10^9$/L)	163.22 ± 15.63	134.11 ± 15.77 [a]	160.67 ± 21.37

[a] Week 12 of treatment (TDF-12) vs. before treatment initiation (baseline, CO) P-value < 0.05. Abbreviations: HBsAg, Hepatitis B surface antigen; HBeAg, hepatitis Be antigen; ALT, Alanine aminotransferase; AST, Aspartate aminotransferase; TBIL, total bilirubin; GGT, Glutamyl transpeptidase; AKP, Alkaline phosphatase; Cr, creatinine; PLT, Platelet.

[b] Week 24 of treatment (TDF-24) vs. before treatment initiation (baseline, CO) P < 0.05.

4.2. Proteomic Profiles of Patients with HBV During TDF Therapy

To characterize the serum protein profiles, we conducted comprehensive QC analyses, including PCA, evaluation of indexed retention time stability, validation of sample intensity, and assessment of quantitative reproducibility (Figure S2). These analyses confirmed that serum sample quality met testing requirements and that the analytical method performed stably. Using DIA-based proteomics, we detected 3170 proteins corresponding to 22,768 peptides using the UniProt human proteome database (Figure 1A and B). Spectronaut software using the Andromeda search engine quantified 1912, 1977, and 1808 proteins in the 3 biological replicates, respectively. From these, a core set of 1540 proteins, representing 48.58% of the total, was consistently identified across all replicates (Figure 1C). To identify differentially expressed proteins, pairwise comparisons of relative protein abundance were conducted among the CO, TDF-12, and TDF-24 groups, revealing 83 proteins (49 upregulated and 34 downregulated) in the TDF-12 group and 104 proteins (63 upregulated and 41 downregulated) in the TDF-24 group compared with the CO group (Figures 2A-E, Tables S1 and S2 in the Supplementary File). Similarly, a comparative analysis of serum samples from the TDF-12 and TDF-24 groups was conducted based on the previously described criteria. Hierarchical clustering analysis revealed 48 differentially expressed proteins, comprising 22 upregulated and 26 downregulated candidates, which distinctly clustered into separate groups (Figure S3A and B and Table S3). The representative differentially expressed proteins consistently identified are listed in Table 2. These findings suggest that molecular mechanisms may differ among the CO, TDF-12, and TDF-24 groups.

To elucidate the functional significance of proteins identified as dysregulated following TDF treatment, KEGG pathway enrichment analysis was performed. Pathway analysis revealed that, compared with the CO group, serum proteins differentially expressed in TDF-12 patients with CHB were primarily associated with autoimmune thyroid disease, Epstein-Barr virus infection, asthma, natural killer cell-mediated cytotoxicity, and allograft rejection, whereas those in TDF-24 patients were mainly enriched in pathways related to human immunodeficiency virus 1 infection, autoimmune thyroid disease, pentose and glucuronate interconversions, Epstein-Barr virus infection, and the PPAR pathway (Figure 2C and F). In contrast, comparison between the TDF-24 and TDF-12 groups showed that dysregulated proteins were mainly involved in regulating glyoxylate and dicarboxylate metabolism, the oxytocin pathway, the nuclear factor kappa B (NF-κB) pathway, platelet activation, and primary immunodeficiency (Figure S3C in the Supplementary File). Thus, these results indicate that specific signaling pathways underlie differences in host macromolecular synthesis between TDF-treated patients and the control group.

4.3. Serum Untargeted Metabolomic Profiling of Patients with HBV During TDF Therapy

Table 2. List of the Typically Differentially Expressed Proteins in Serum Samples from Patients with CHB Following Treatment with Tenofovir Disoproxil Fumarate (TDF)

Protein accession	Protein description	Gene Name	Fold Change		
			TDF-12 vs CO	TDF-24 vs CO	TDF-24 vs TDF-12
P09912	Interferon alpha-inducible protein 6	IFI6	2.67	4.47	1.67
O15145	Actin-related protein 2/3 complex subunit 3	ARPC3	2.11	4.00	1.90
Q9NQ30	Endothelial cell-specific molecule 1	ESM1	2.43	3.20	1.32
Q5JRA6	Transport and Golgi organization protein 1 homolog	MIA3	2.22	2.94	1.33
P55157	Microsomal triglyceride transfer protein large subunit	MTTP	1.19	2.78	2.34
O00468	Agrin	AGRN	2.46	2.74	1.11
P0C0L4	Complement C4-A	C4A	1.78	2.53	1.43
P61769	Beta-2-microglobulin	B2M	1.77	2.51	1.42
P00326	Alcohol dehydrogenase 1C	ADH1C	1.03	2.33	2.26
P02763	Alpha-1-acid glycoprotein 1	ORM1	2.27	2.23	0.98
P08833	Insulin-like growth factor-binding protein 1	IGFBP1	1.56	2.17	1.39
P19971	Thymidine phosphorylase	TYMP	1.88	2.09	1.11
Q9BRK5	45 kDa calcium-binding protein	SDF4	1.52	2.09	1.37
Q08380	Galectin-3-binding protein	LGALS3BP	2.28	2.00	0.87
Q01469	Fatty acid-binding protein 5	FABP5	1.62	1.94	1.20
P02787	Serotransferrin	TF	1.80	1.91	1.06
Q8NDI1	EH domain-binding protein 1	EHBP1	0.44	0.31	0.71
P11678	Eosinophil peroxidase	EPX	0.44	0.32	0.72
Q684P5	Rap1 GTPase-activating protein 2	RAP1GAP2	0.27	0.33	1.24
P29279	CCN family member 2	CCN2	0.78	0.50	0.64
Q14831	Metabotropic glutamate receptor 7	GRM7	0.78	0.52	0.66
O43852	Calumenin	CALU	0.56	0.52	0.94
Q9BQI4	Coiled-coil domain-containing protein 3	CCDC3	0.59	0.57	0.97
Q6Q788	Apolipoprotein A-V	APOA5	0.62	0.57	0.92
P07093	Glia-derived nexin	SERPINE2	0.67	0.60	0.89
O94907	Dickkopf-related protein 1	DKK1	0.66	0.61	0.92

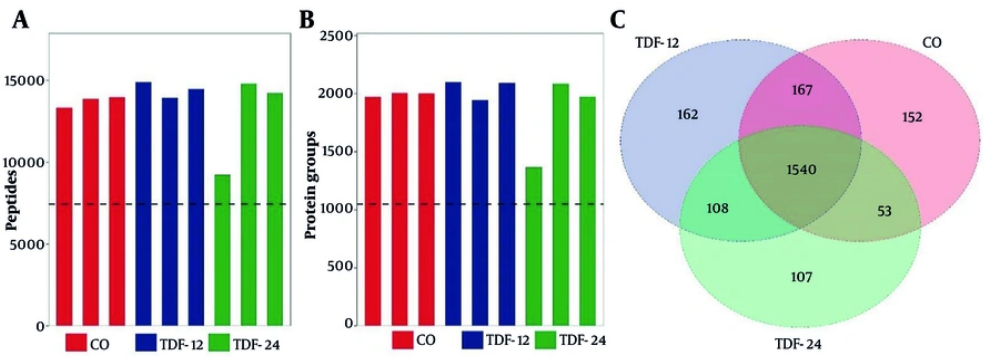

Figure 1. Profiling of the serum proteome in patients with HBV at baseline (CO) and after 12 (TDF-12) and 24 (TDF-24) weeks of TDF therapy. (A) Peptides identified in each replicate. (B) Protein groups identified in each replicate. (C) Overlap of proteins consistently quantified among the three groups.

Untargeted metabolomic analysis was performed on serum samples across 3 experimental groups using both positive and negative ionization modes. To validate the reliability of the untargeted metabolomics data, we

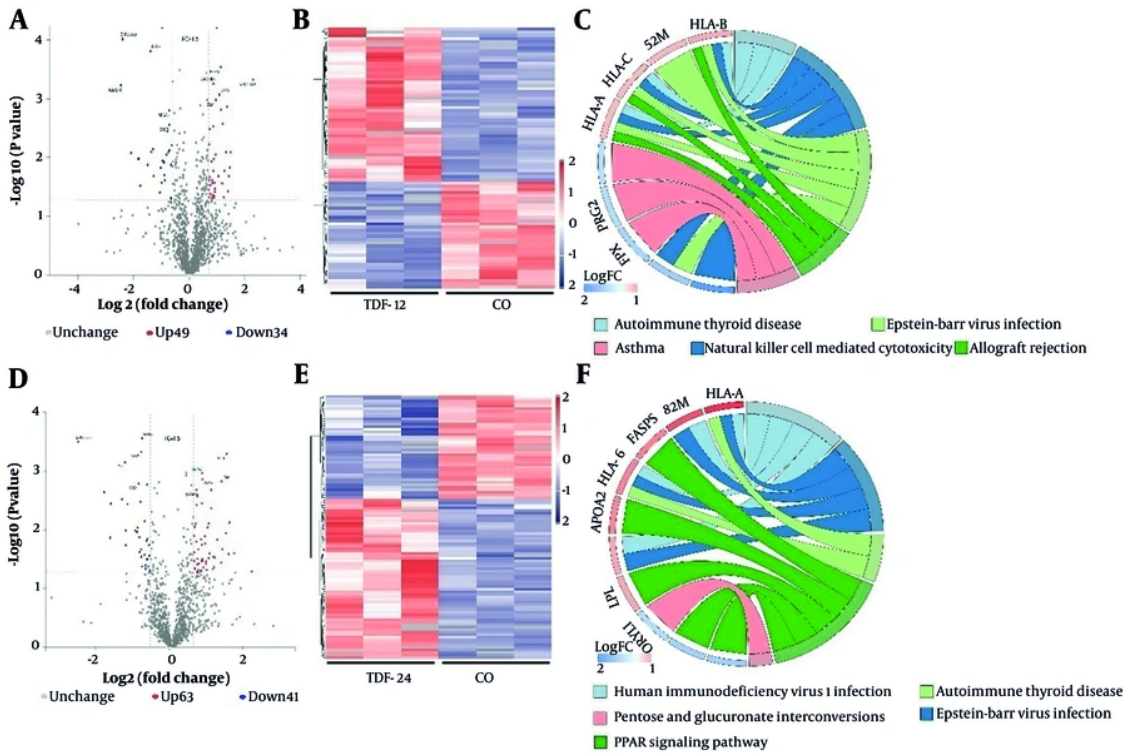

Figure 2. Bioinformatic characterization of serum proteome changes during TDF treatment by comparing the 12-week (TDF-12) and 24-week (TDF-24) groups against baseline (CO). (A) Volcano plot of differential protein abundance (CO vs. TDF-12), identifying 83 dysregulated proteins. (B) Hierarchical clustering of the 83 dysregulated proteins (CO vs. TDF-12). (C) KEGG pathway enrichment analysis (chord diagram) for proteins dysregulated in CO vs. TDF-12. (D) Volcano plot of differential protein abundance (CO vs. TDF-24), identifying 104 dysregulated proteins. (E) Hierarchical clustering of the 104 dysregulated proteins (CO vs. TDF-24). (F) KEGG pathway enrichment analysis (chord diagram) for dysregulated proteins (CO vs. TDF-24).

conducted comprehensive QC analyses on all samples (Figure S4 in the Supplementary File). These analyses collectively confirmed robust experimental reproducibility, acceptable instrument performance variability, and the suitability of the dataset for downstream analytical procedures. Matching UPLC-Q-TOF MS/MS data against the compound database yielded 21,874 serum features, including 10,380 in positive mode and 11,493 in negative mode (Figure 3A). After integration of the datasets from both positive and negative ionization modes, the identified metabolites were systematically classified into chemical taxonomy groups using Human Metabolome Database annotations. The majority were lipids and lipid-like molecules (31.398%), followed by organic acids and derivatives (20.079%), benzenoids (11.516%), and organoheterocyclic compounds (10.827%) (Figure 3B).

To identify differentially expressed serum metabolites, the relative abundances of metabolites in the TDF treatment groups were compared with those in the CO control group (Figure 3C). The serum metabolite profiles were further investigated through systematic analysis of the differentially expressed metabolites, using correlation analysis and clustering heatmaps based on Pearson correlation coefficients to identify the most strongly correlated and uncorrelated metabolite pairs. Hierarchical clustering and KEGG enrichment analysis identified 101 differentially expressed metabolites in the TDF-12 group compared with CO controls (32 upregulated and 69 downregulated), enriched in pathways such as the cAMP signaling pathway and arginine and proline metabolism (Figure 4A-C and Table S4 in the Supplementary File), and 105 differentially expressed metabolites in the TDF-24 group compared with CO controls (60 upregulated and 45 downregulated), primarily associated with propanoate metabolism, glycine, serine and threonine metabolism, and general metabolic pathways (Figure 4D-F and Table S5 in the Supplementary File). In addition, comparison between the TDF-24 and TDF-12 groups revealed 84

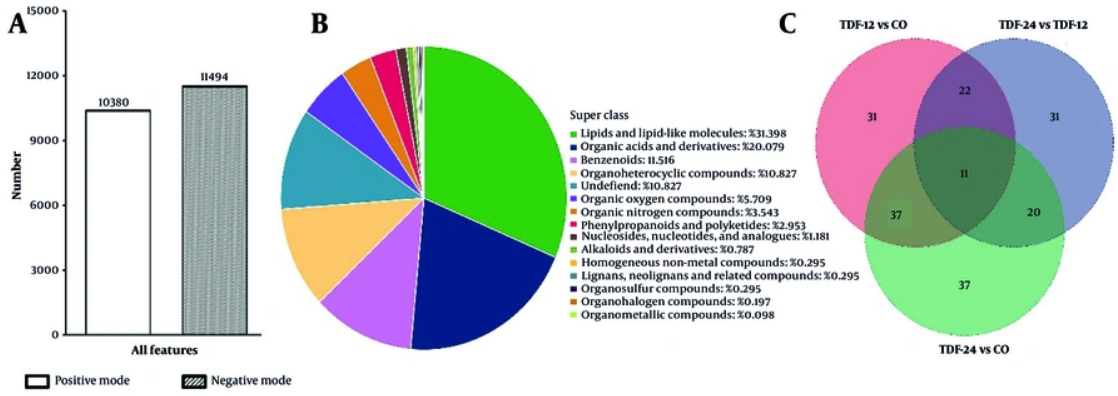

Figure 3. Identification of serum metabolites in patients with CHB before treatment initiation (baseline, CO), at week 12 of treatment (TDF-12), and at week 24 of treatment (TDF-24). (A) Features identified in metabolomic analysis. (B) Venn diagram showing the overlap of identified metabolites among the three groups. (C) Chemical classification of the differentially expressed metabolites.

Table 3. List of the Typically Differentially Expressed Metabolites in Serum Samples from Patients with CHB Following Treatment with Tenofovir Disoproxil Fumarate (TDF)

Metabolite ID	Adducted form	Metabolite Name	TDF-12 vs CO	TDF-24 vs CO	TDF-24 vs TDF-12
M367T170	[M-H]-	2,2'-methylene-bis(6-tert-butyl)-4-ethylphenol	1.73	4.96	2.87
M187T24_1	[M-H]-	2,4-diaminobenzenesulfonic acid	2.24	5.14	2.30
M153T24	[M-H]-	2,6-dihydroxybenzoic acid	1.74	3.22	1.85
M178T211	[M-H-CH3]-	3-hydroxy-4-methoxycinnamic acid	2.52	3.92	1.56
M397T50	[M-H-C7H12O4]-	Atorvastatin	1.39	1.83	1.32
M182T320	[M+Na]+	Betonicine	10.78	10.65	0.99
M173T24_1	[M-H-H2O]-	Isocitric acid	1.54	1.91	1.25
M339T193	[M-H]1-	Leukotriene b4	1.18	1.62	1.38
M443T31	[M-H]-	Mitoxantrone	1.40	2.09	1.50
M439T58	[M-H-C7H15NO7]-	Natamycin	6.31	7.41	1.17
M93T24	[M-H]-	Phenol	1.50	2.12	1.41
M263T244	[M-H]-	Phenylacetyl-l-glutamine	1.30	1.98	1.52
M515T104	[M+H]+	Telmisartan	76.32	135.69	1.78
M101T120	[M-H]-	2-ketobutyric acid	0.63	0.45	0.71
M103T253	[M-H]-	3-hydroxybutyric acid	0.18	0.09	0.51
M187T101	[M-H]-	3-hydroxycapric acid	0.48	0.43	0.90
M103T216	[M-H]-	Dl-a-hydroxybutyric acid	0.46	0.38	0.82
M137T188	[M+H]+	Hypoxanthine	0.60	0.41	0.68
M267T240	[M-H]-	Inosine	0.24	0.10	0.42
M275T31	[M-H]-	Menthyl salicylate	0.52	0.49	0.94
M123T53	[M-H]-	Orcinol	0.50	0.43	0.86
M175T349	[M-H]-	Ser-Ala	0.51	0.33	0.65
M227T310	[M-H]-	Trans-traumatic acid	0.12	0.14	1.23

differentially expressed metabolites (56 upregulated and 28 downregulated), with predominant enrichment in the cAMP signaling pathway (Figure S5 and Table S6 in the Supplementary File). The characteristic differentially expressed metabolites are summarized in Table 3. Collectively, the serum untargeted metabolomic signatures observed in patients with CHB across distinct durations of TDF treatment suggest treatment duration-

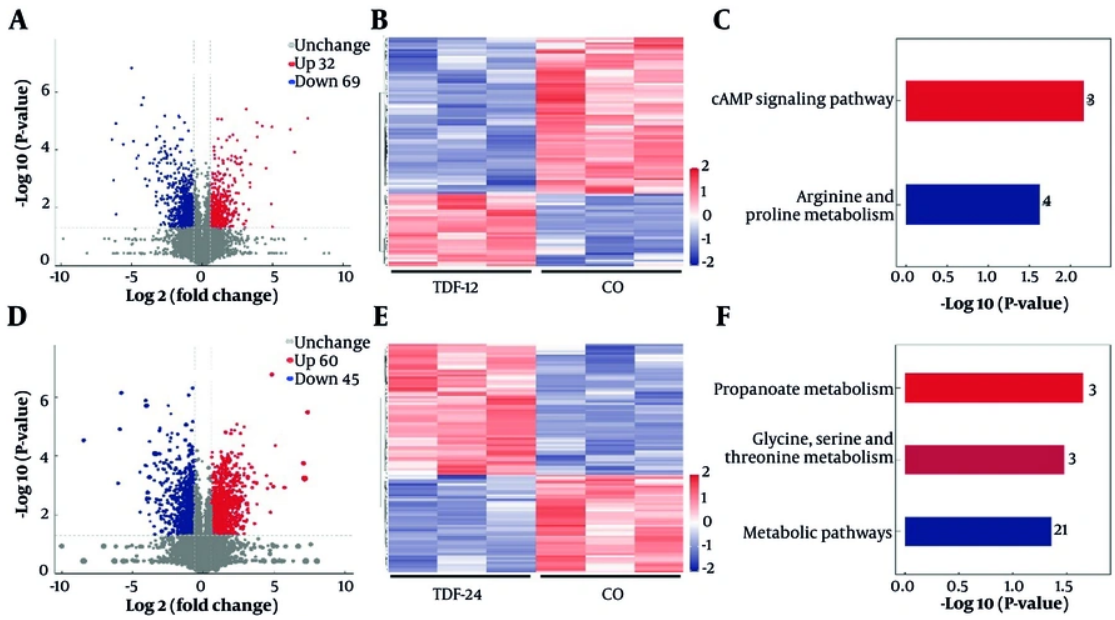

Figure 4. Bioinformatics analysis of differentially expressed serum metabolites. Analyses compare the week 12 of treatment (TDF-12) and week 12 of treatment (TDF-12) treatment groups against the baseline control (CO) group. (A) Volcano plot of metabolite abundance changes between the CO and TDF-12 groups. (101 dysregulated metabolites). (B) Hierarchical clustering of the 101 dysregulated metabolites (CO vs. TDF-12). (C) Bar chart of KEGG pathway enrichment for dysregulated metabolites (CO vs. TDF-24). (D) Volcano plot of metabolite abundance changes between the CO and TDF-24 groups (105 dysregulated metabolites). (E) Hierarchical clustering of the 105 dysregulated metabolites (CO vs. TDF-24). (F) Bar chart of KEGG pathway enrichment for dysregulated metabolites (CO vs. TDF-24).

dependent metabolic reprogramming, which may underlie the pathogenesis and progression of disease under antiviral therapy.

4.4. Pathway Analysis Integrating Proteomic and Metabolomic Data from Patients with CHB During TDF Therapy

To investigate potential synergistic interactions between dysregulated proteins and metabolites within biological pathways, we performed integrated KEGG pathway enrichment analysis of both omics datasets, identifying pathways that were concurrently enriched at both the proteomic and metabolomic levels. KEGG pathway analysis revealed that, compared with the CO control group, the TDF treatment groups exhibited distinct enrichment patterns at different stages. The TDF-12 group showed significant dysregulation in pathways including neurodegeneration-multiple diseases, regulation of the actin cytoskeleton, diabetic cardiomyopathy, the cAMP signaling pathway, and biosynthesis of cofactors (Figure 5A), whereas the TDF-24 group exhibited alterations in the PPAR signaling pathway, purine metabolism, biosynthesis of cofactors, chemical carcinogenesis-reactive oxygen species, tyrosine metabolism, nucleotide metabolism, and the cAMP signaling pathway (Figure 5B). Compared with the TDF-12 group, the TDF-24 group showed significant enrichment in regulation of the actin cytoskeleton, pathways of neurodegeneration-multiple diseases, the cAMP pathway, pancreatic secretion, and diabetic cardiomyopathy (Figure S5 in the Supplementary File). Notably, integrated pathway analysis showed that the PPAR pathway was the most significantly enriched pathway at the prespecified virologic response endpoint (week 24, with HBV DNA < 30 IU/mL). This finding suggests its potential role in the pathogenesis and disease progression of patients with CHB under varying durations of TDF-based antiviral therapy.

4.5. Validation of Selected Differentially Expressed Proteins and Metabolites

Integrating the results from hierarchical clustering (Figure 2 and 4) and key signaling pathways (Figure 6), the proteins fatty acid-binding protein 5 (FABP5) and apolipoprotein A-V (APOA5), as well as the metabolites 3-hydroxybutyric acid (BHB) and leukotriene B4 (LTB4), exhibited distinct expression patterns between the TDF treatment groups (TDF-12 and TDF-24) and the CO

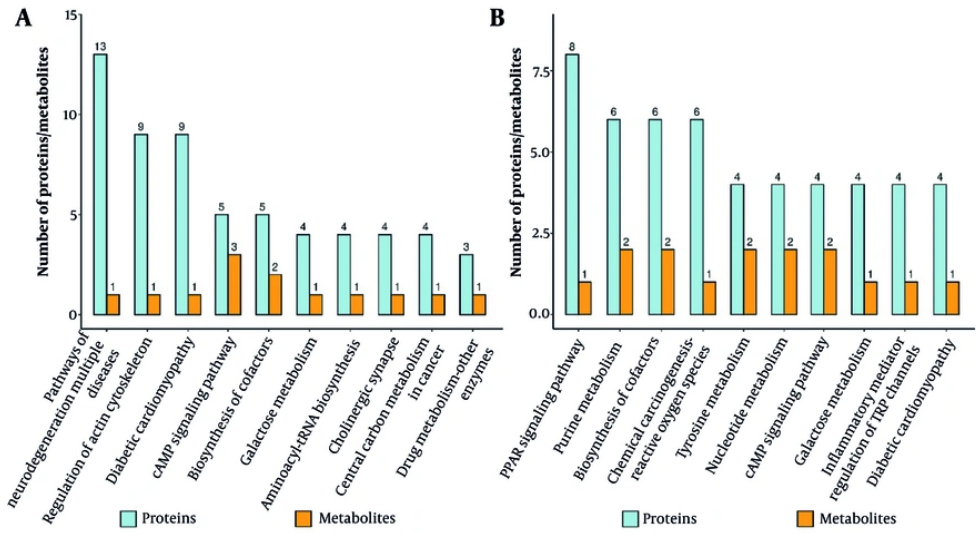

Figure 5. Bar chart of top enriched KEGG pathways based on differential proteins and metabolites at baseline (CO), 12 weeks (TDF-12), and 24 weeks (TDF-24) of TDF treatment. (A) CO group versus TDF-12 group. (B) CO group versus TDF-24 group.

control group. Therefore, differential expression of proteins (FABP5 and APOA5) and metabolites (BHB and LTB4) under TDF-based antiviral treatment in patients with CHB may form therapy-specific regulatory networks that govern key biological processes and molecular functions, potentially through modulation of the PPAR pathway. Accordingly, to validate the proteomic and metabolomic findings, we quantitatively analyzed serum levels of the key regulatory factors (FABP5, APOA5, BHB, and LTB4) using ELISA in a cohort comprising 54 samples divided into 3 HBV groups: CO control (n = 18), TDF-12 (n = 18), and TDF-24 (n = 18). Consistent with our multi-omics analyses, Figure 7 shows that TDF treatment significantly downregulated APOA5 and BHB and upregulated FABP5 and LTB4 relative to CO controls. These findings strongly suggest that aberrant expression of proteins and metabolites may critically affect disease progression in patients with CHB receiving varying durations of TDF-based antiviral therapy, potentially via modulation of the PPAR signaling pathway, although the precise underlying molecular mechanisms require further elucidation.

To further evaluate the diagnostic potential of the identified differentially expressed proteins (APOA5 and FABP5) and metabolites (BHB and LTB4) in patients with CHB across different TDF treatment stages and controls, we performed ROC curve analysis (Figure 8). The analysis demonstrated that the candidate molecules exhibited strong discriminatory ability. In distinguishing the TDF-12 group from the CO group, both proteins and metabolites showed near-perfect performance. Specifically, APOA5 (AUC = 0.998) and FABP5 (AUC = 0.971), along with BHB (AUC = 0.996) and LTB4 (AUC = 0.957), all achieved extremely high AUC values, with sensitivity and specificity exceeding 91.67% and 86.11%, respectively. Excellent diagnostic performance was also observed in distinguishing the TDF-24 group from the CO group. Similarly, when comparing the TDF-24 group with the CO group, these candidate molecules continued to display strong predictive capabilities. In contrast, FABP5 showed limited ability to distinguish TDF-24 from TDF-12, as reflected by a lower AUC and lack of statistical significance ($P > 0.05$). Ultimately, this exploratory ROC analysis provides preliminary evidence that regulation of the PPAR pathway could help distinguish patients at different TDF treatment stages, suggesting its potential role in the host response. However, this requires validation in larger independent cohorts.

5. Discussion

Although HBV remains globally prevalent and continues to pose a major public health threat through associated liver diseases, including cirrhosis, liver failure, and HCC, the incidence of chronic HBV infection has declined, largely because of advances in antiviral therapy and the widespread implementation of

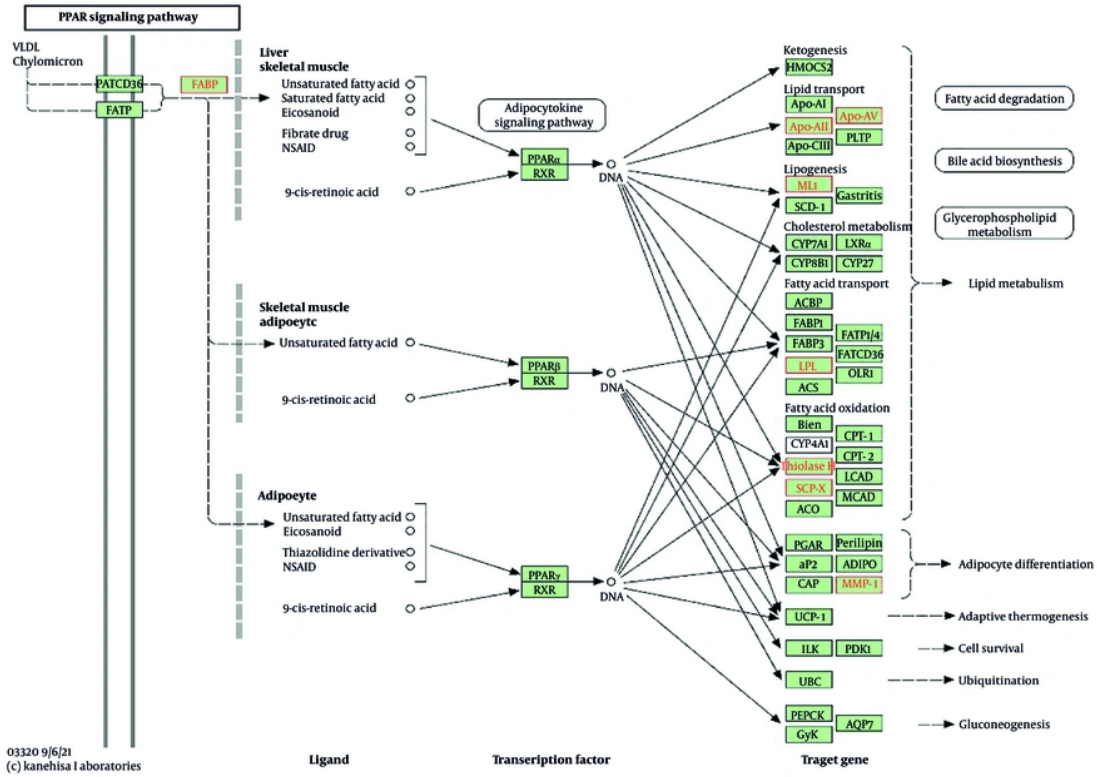

Figure 6. Schematic of the PPAR pathway, highlighted based on integrated KEGG pathway enrichment analysis of proteins and metabolites dysregulated in chronic hepatitis B (CHB) patients after 12 weeks of TDF treatment (TDF-12) and 24 weeks of TDF treatment (TDF-24).

vaccination programs (4, 5). In HBV treatment, the primary goal is a clinical cure, defined by HBsAg clearance, potential hepatitis B surface antibody seroconversion, and HBV DNA suppression below detection, with NAs central to antiviral therapy (1, 6). Accumulated evidence confirms that TDF effectively inhibits HBV reverse transcription and reduces viral replication. Furthermore, long-term TDF treatment, particularly in inactive HBsAg carriers with low baseline HBsAg levels, can reactivate functionally impaired immune cells by reducing viral antigen load, thereby restoring HBV-specific immune function and promoting the establishment of a dominant immune population conducive to functional cure (7, 9, 10). Nevertheless, the specific biochemical mechanisms underlying TDF-mediated functional cure, encompassing both its direct antiviral effects and indirect immunomodulatory effects on the host, remain incompletely understood. To the best of our knowledge, this study is the first to characterize serum proteomic and metabolomic profiles following TDF therapy in patients with CHB. The identification of these molecular changes offers novel insights and generates testable hypotheses regarding the mechanisms underlying TDF treatment-induced functional cure.

To elucidate the mechanisms underlying CHB pathogenesis during TDF therapy and identify novel therapeutic targets, we systematically investigated concomitant proteomic and metabolomic alterations in serum using the same set of patient samples. In this study, we used an integrated platform of DIA-MS and UHPLC-Q-Orbitrap MS/MS to perform comprehensive proteomic and metabolomic profiling of serum samples from 3 cohorts (CO control, TDF-12, and TDF-24), capturing dynamic changes associated with clinically relevant TDF therapy. Based on predefined criteria for differential expression, comparative analysis with CO controls identified 83 dysregulated proteins and 101 dysregulated metabolites in the TDF-12 group, and 104 dysregulated proteins and 105 dysregulated metabolites

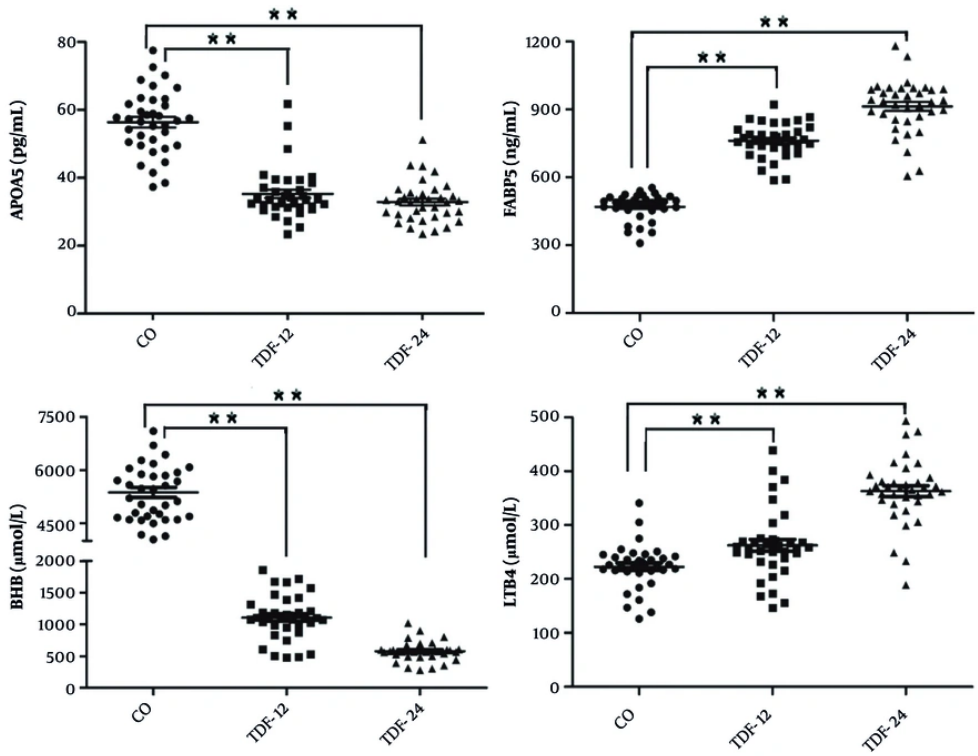

Figure 7. Verification of serum protein and metabolite expression in chronic hepatitis B (CHB) patients at baseline (CO) and after 12 (TDF-12) and 24 (TDF-24) weeks of tenofovir disoproxil fumarate (TDF) treatment. Differential expression was confirmed by enzyme-linked immunosorbent assay (ELISA). Data are presented as mean ± SEM (n = 18; *P < 0.05, **P < 0.01).

in the TDF-24 group, indicating that CHB pathogenesis during TDF therapy involves distinct stage-specific molecular mechanisms (Figures 2 and 4). Although the dysregulated proteins and metabolites were linked to multiple signaling pathways integral to HBV infection under TDF therapy, the integrated proteomic and metabolomic data showed the most significant enrichment in the TDF-24 group. This molecular signature was specifically associated with achievement of the prespecified virologic response endpoint. These findings suggest that, in patients with CHB receiving TDF treatment, the PPAR pathway may critically modulate clinical features and disease progression, positioning it as a potential novel therapeutic target for CHB during TDF treatment.

The PPAR pathway, which comprises a family of nuclear receptor transcription factors (PPARα, PPARγ, and PPARβ/δ), plays a critical role in regulating lipid metabolism, inflammatory responses, and cell proliferation (26, 27). Despite significant differences in structure, tissue distribution, and function, all 3 isoforms are involved in essential physiological processes, such as cellular metabolic homeostasis, proliferation, differentiation, and inflammatory regulation (26-28). PPARα is predominantly expressed in the liver and primarily regulates fatty acid oxidation and energy metabolism, whereas PPARγ is mainly localized in adipose tissue and immune cells, where it contributes to adipogenesis and modulation of inflammation, and PPARβ/δ is widely distributed across tissues and modulates lipid metabolism and cell proliferation (26-28). In the context of HBV infection, PPARα serves as a key regulator of lipid metabolism and viral transcription by forming a heterodimer with retinoid X receptor α to activate the HBV core promoter and enhance pregenomic RNA transcription. Its activation via the PGC-1α/PPARα/SIRT1 axis upregulates hepatocyte nuclear factor 4α, further facilitating viral replication, whereas HBV infection-induced pyruvate production suppresses PPARα expression, leading to reactive oxygen species accumulation and extracellular matrix gene upregulation, ultimately promoting the

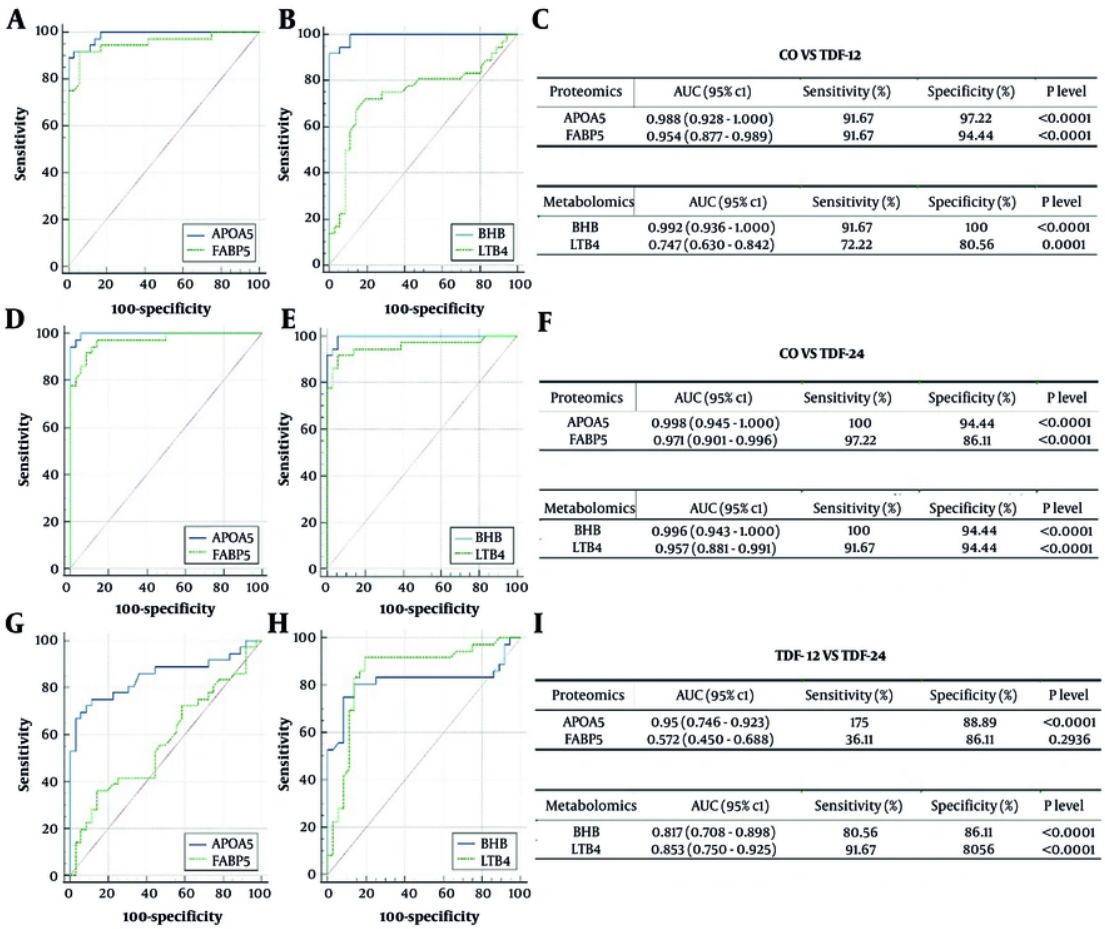

Figure 8. Diagnostic performance of candidate protein and metabolite molecules for distinguishing chronic hepatitis B (CHB) patients at baseline (before treatment initiation, CO), 12 weeks after tenofovir disoproxil fumarate (TDF) treatment (TDF-12), and 24 weeks after TDF treatment (TDF-24). A, D, G, ROC curves for proteomic models (APOA5/FABP5) in pairwise TDF time-point comparisons (CO vs. TDF-12; CO vs. TDF-24; TDF-12 vs. TDF-24); B, E, H, ROC curves for metabolomic models (BHB/LTB4) in the same pairwise comparisons; C, F, I, Performance metrics (AUC, Sensitivity, Specificity, P-value) for proteomic/metabolomic models in CO vs. TDF-12, CO vs. TDF-24, and TDF-12 vs. TDF-24 comparisons, respectively.

development of hepatic fibrosis (28-30). In addition, in a mouse model of HBV-induced hepatic fibrosis, targeted adeno-associated virus short hairpin RNA therapy upregulates PPARγ expression and inhibits nuclear factor-κB p65 phosphorylation and α-smooth muscle actin, thereby alleviating liver inflammation. This finding demonstrates the crucial anti-inflammatory and protective role of PPARγ activation in the liver through mechanisms such as suppression of proinflammatory pathways, modulation of immune cell functions, and improvement of lipid metabolism (30). Our results suggest that the clinical manifestations of HBV under TDF therapy are largely driven by the activity level of the PPAR pathway, thereby accounting for the pathway involvement observed in both groups.

Compared with the CO group, serum APOA5 and FABP5 levels in the TDF-12 and TDF-24 patient groups exhibited significant and sustained downregulation and upregulation trends, respectively, suggesting their involvement in the pathophysiological mechanisms of TDF treatment for HBV. APOA5, a liver-synthesized protein positively regulated by PPARα, ameliorates hepatic lipid metabolism disorders by promoting lipid breakdown and suppressing hepatocellular triglyceride synthesis via lipoprotein lipase activation and very-low-density lipoprotein secretion (31, 32). Its downregulation impairs the nuclear translocation and transcriptional

activation of PPARα, thereby reducing the expression of downstream target genes, such as CPT1A, ACOX1, and ACADL, that are essential for mitochondrial and peroxisomal β-oxidation (30, 32). In addition, FABP5 primarily mediates the intracellular transport and signaling of long-chain fatty acids and modulates PPARγ activity to promote macrophage polarization toward an M2 immunoregulatory phenotype, thereby reshaping the hepatic immune microenvironment (33, 34). Upregulation of FABP5 establishes a critical signaling node by mediating crosstalk between the PPARγ activation pathway and NF-κB-driven inflammatory responses, thereby fine-tuning cellular outcomes between metabolic regulation and inflammation (35). The results of this study demonstrated that TDF treatment modulates host lipid metabolism in HBV-infected patients through a dual mechanism. This process is initiated by activation of PPARα, which is restored as TDF reduces viral load and alleviates infection-mediated suppression of PPARα activity. Consequently, this restoration directly downregulates the expression of its target gene, APOA5; the proposed mechanism is that antiviral therapy suppresses PPARα signaling, leading to APOA5 downregulation, inhibition of lipoprotein lipase activity, and/or reduced very-low-density lipoprotein secretion, ultimately impairing triglyceride clearance and elevating plasma triglyceride levels. This provides a mechanistic explanation for the dyslipidemia observed in some patients with CHB after prolonged antiviral treatment. Concurrently, attenuation of hepatic inflammation following viral suppression leads to activation of PPARγ, which upregulates FABP5. This upregulation suppresses NF-κB p65 phosphorylation and α-smooth muscle actin expression, thereby ultimately mitigating the progression of HBV-related liver disease.

In the nontargeted metabolomics analysis of serum, HBV samples from the TDF group exhibited significant downregulation of BHB and upregulation of LTB4 compared with the CO group, suggesting an imbalance in the PPAR signaling pathway. BHB, an endogenous ketone body metabolite, has been demonstrated to modulate hepatic pathology indirectly through PPAR pathways via mechanisms such as metabolic substrate supply, epigenetic modification, or receptor crosstalk (36, 37). This includes its precursor acetoacetate targeting PPARγ to restore lipid droplet storage in hepatic stellate cells and inhibit their activation, thereby slowing liver fibrosis progression, as well as BHB downregulation regulating the expression of genes involved in fatty acid activation, transport, and β-oxidation in subcutaneous adipose tissue through the PPAR signaling pathway to suppress fatty acid oxidation and lipid remodeling (37, 38). LTB4, a key inflammatory mediator generated via 5-lipoxygenase-catalyzed fatty acid metabolism, plays a pivotal role in immune regulation through its dual functions: Exerting potent proinflammatory and chemotactic effects by binding to the cell-surface receptors LTB4 receptor 1 and LTB4 receptor 2, and serving as a signaling molecule that activates the nuclear receptor PPARα in immune cells (39, 40). Once activated, PPARα reciprocally suppresses LTB4 release and accelerates its catabolism, thereby attenuating proinflammatory activity and promoting inflammation resolution, forming a critical LTB4-PPARα signaling axis that bridges lipid metabolism and immune inflammation (40).

It is important to emphasize that the candidate molecular patterns identified in this discovery-phase study are derived from, and therefore primarily relevant to, a specific cohort: Treatment-naïve patients with CHB who achieved a sustained virologic response after 24 weeks of TDF monotherapy. In the current study, we identified dysregulation of several proteins and metabolites, including APOA2, FABP5, BHB, and LTB4. These molecules are functionally associated with the PPAR signaling pathway. Their coordinated changes suggest a potential regulatory role for this pathway in HBV-related liver diseases during TDF therapy, possibly mediated through modulation of serum protein and metabolite levels. Consequently, the expression levels of these differentially regulated molecules represent candidate biomarkers that merit further investigation for distinguishing HBV-infected patients undergoing TDF therapy. Moreover, these serum protein and metabolite markers represent candidate targets for further investigation in TDF-treated HBV infection, with the potential to inform improved prevention and management strategies for HBV and its associated liver diseases. However, the precise mechanisms through which they regulate the PPAR signaling pathway remain incompletely understood and require further investigation.

Overall, this integrated proteomic and metabolomic investigation elucidated key pathophysiological effects of HBV infection under TDF treatment. The study provides novel mechanistic insights that substantially advance our understanding of HBV-related disease mechanisms during TDF therapy. Our results underscore the PPAR signaling pathway as a promising therapeutic target for TDF-treated HBV-driven liver diseases, potentially accessible through intervention targeting key associated proteomic and metabolic molecules.

5.1. Study Limitations

Several limitations of this study warrant consideration. First, our study was constrained by a relatively limited sample size, which may affect the broader applicability of the results. Second, the lack of comprehensive multi-omics data in CHB research has hindered a more integrated view of its molecular mechanisms. Third, the longitudinal molecular signatures identified in this study, particularly those involving the PPAR pathway and associated molecules such as FABP5, APOA5, BHB, and LTB4, are discovery-phase candidates rather than validated biomarkers. No diagnostic panel with defined cutoffs was established. Moreover, as an exploratory study, we did not apply formal multiple-testing correction, and the ROC analysis was performed internally. These methodological approaches, while appropriate for initial discovery, increase the risk of false-positive findings and overfitting. Future studies with larger independent cohorts are necessary to translate these exploratory findings into a formal diagnostic assay. Finally, despite stringent experimental controls, inherent technical variations in serum proteomic and metabolomic methodologies may introduce confounding factors, potentially complicating data interpretation.

5.2. Conclusion

In this study, we used an integrated multi-omics approach to investigate serial serum samples from patients with CHB at CO, TDF-12, and TDF-24. This comprehensive analysis identified unique protein and metabolite signatures associated with CHB, characterized their expression profiles and coregulatory networks, and revealed a crucial role for dysregulated PPAR signaling in the pathogenesis of HBV infection among patients receiving TDF treatment. As expected, serum proteomic and metabolic profiles differed across TDF treatment stages in patients with CHB, indicating distinct host cellular reprogramming at TDF-12 and TDF-24. Using consistent omics platforms, we reproducibly identified 2 proteins (FABP5 and APOA5) and 2 metabolites (LTB4 and BHB) that are functionally linked to the PPAR signaling pathway. In summary, this study delineates molecular differences in HBV-infected individuals during TDF treatment and suggests that PPAR pathway-associated molecules, such as FABP5, APOA5, LTB4, and BHB, represent candidate biomarkers and hypothetical therapeutic targets worthy of further investigation in treatment-naïve patients responding to TDF monotherapy. These findings generate hypotheses for therapeutic targeting and provide a molecular foundation for future research aimed at developing validated diagnostic or monitoring panels. No formal clinical test was defined in this initial investigation.

Supplementary Material

Supplementary material(s) is available here [To read supplementary materials, please refer to the journal website and open PDF/HTML].

Footnotes

AI Use Disclosure: The authors declare that no generative AI tools were used in the creation of this article.

Authors' Contribution: Peixia Lin contributed to formal analysis, methodology, validation, and writing the original draft. Zhaojun Jin contributed to formal analysis, methodology, and investigation. Yimin Chen and Jiaxin Jin contributed to formal analysis and investigation. Min Deng contributed to conceptualization, supervision, and resources. Dahai Wei contributed to conceptualization, project administration, supervision, review and editing, and resources.

Conflict of Interests Statement: The authors declare that they have no conflicts of interest or personal relationships.

Data Availability: All data generated during this study are included in this published article. The mass spectrome-try proteomics data have been deposited to the ProteomeXchange Consortium (https://proteomecentral.proteomexchange.org) via the iProX partner repository with the dataset identifier PXD073035.

Ethical Approval: This research was conducted in strict accordance with the study design, reviewed and approved by the Institutional Ethics Committee of Affiliated Hospital of Jiaxing University (ethics approval number 2023-LY-519) and adheres strictly to the tenets of the Declaration of Helsinki. Written informed consent was obtained from the study participants prior to study commencement.

Funding/Support: This work was supported by Zhejiang Provincial Natural Science Foundation of China under Grant No. LTGY24C010001, Jiaxing Key Laboratory of Virus-related Infectious Disease, and 2023 Jiaxing Key Discipline of Medcine-Lemology (Supporting Subject, Grant No. 2023-ZC-009).

Informed Consent: Written informed consent was obtained from the study participants prior to study commencement.

References

1. Feld JJ, Gehring AJ, Zoulim F. Getting to HBV cure-Will new biomarkers help? *Hepatology*. 2025;**10**:1097. [PubMed ID: 40168396]. https://doi.org/10.1097/HEP.0000000000001334.
2. Kennedy PT, Allweiss L, Bertoletti A, Cornberg M, Gehring AJ, Guidotti LG, et al. Scientific and medical evidence informing expansion of hepatitis B treatment guidelines. *Lancet Gastroenterol Hepatol*. 2025;**10**(10):941-951. [PubMed ID: 40714040]. [PubMed Central ID: PMC12797741]. https://doi.org/10.1016/S2468-1253(25)00053-6.
3. Stockdale AJ, Holt B, Bhadoria AS, Sadasivan A, Ikeda D, Pollack T, et al. Service delivery models and care cascade outcomes for people living with chronic hepatitis B: a global systematic review and meta-analysis. *Lancet Gastroenterol Hepatol*. 2025;**10**(11):1013-1027. [PubMed ID: 40819651]. https://doi.org/10.1016/S2468-1253(25)00163-3.
4. Mak LY, Huang DQ. Novel insights into chronic HBV infection. *Nat Rev Gastroenterol Hepatol*. 2026;**23**(2):122-123. [PubMed ID: 41407874]. https://doi.org/10.1038/s41575-025-01163-8.
5. Papatheodoridi M, Tampaki M, Lok AS, Papatheodoridis GV. Risk of HBV reactivation during therapies for HCC: a systematic review. *Hepatology*. 2022;**75**(5):1257-1274. [PubMed ID: 34918361]. https://doi.org/10.1002/hep.32241.
6. Ghany MG, Pan CQ, Lok AS, Feld JJ, Lim JK, Wang SH, et al. AASLDIDSA Practice Guideline on treatment of chronic hepatitis B. *Hepatology*. 2026;**83**(4):974-997. [PubMed ID: 41186418]. https://doi.org/10.1097/HEP.0000000000001549.
7. Lim SG, Baumert TF, Boni C, Gane E, Levrero M, Lok AS, et al. The scientific basis of combination therapy for chronic hepatitis B functional cure. *Nat Rev Gastroenterol Hepatol*. 2023;**20**(4):238-253. [PubMed ID: 36631717]. https://doi.org/10.1038/s41575-022-00724-5.
8. Yucuma D, Rakover A, Warsop ZI, Im YR, Chen SE, Jagdish R, et al. Natural history of chronic hepatitis B in untreated adults without cirrhosis according to baseline hepatitis B virus DNA and alanine aminotransferase concentrations: a systematic review and meta-analysis. *Lancet Gastroenterol Hepatol*. 2026;**11**(5):380-396. [PubMed ID: 41839199]. https://doi.org/10.1016/S2468-1253(25)00302-4.
9. Chen Y, Deng M, Tong M, Lin P, Xuan H, Wei D. A study on serum protein tracking in patients with low levels of HBsAg undergoing treatment for chronic hepatitis B with a combination of tenofovir disoproxil fumarate and pegylated interferon. *Hepat Mon*. 2025;**25**(1). e165660. https://doi.org/10.5812/hepatmon-165660.
10. Samadi Kochaksaraei G, Shaheen AA, Seow CH, Barkema HW, Coffin CS. Tenofovir disoproxil fumarate therapy to prevent hepatitis B virus vertical transmission-A review of maternal and infant outcomes. *Liver Int*. 2022;**42**(8):1712-1730. [PubMed ID: 35312156]. https://doi.org/10.1111/liv.15249.
11. Scott LJ, Chan HLY. Tenofovir alafenamide: a review in chronic hepatitis B. *Drugs*. 2017;**77**(9):1017-1028. [PubMed ID: 28493172]. https://doi.org/10.1007/s40265-017-0754-9.
12. Chen J, Lai S, Zheng M. Efficacy analysis and influencing factors of HBsAg response in chronic hepatitis B patients treated with nucleoside analogues and pegylated interferon sequential therapy with high HBsAg levels. *Hepat Mon*. 2025;**25**(1). e165180. https://doi.org/10.5812/hepatmon-165180.
13. Rodrigo M, Hartley C, Wasuwanich P, Van T, Karnsakul W. From tenofovir disoproxil fumarate (TDF) to tenofovir alafenamide (TAF): perspectives in pediatric patients with chronic hepatitis B. *Expert Rev Anti Infect Ther*. 2024;**22**(12):1099-1106. [PubMed ID: 39360716]. https://doi.org/10.1080/14787210.2024.2412991.
14. Byun KS, Choi J, Kim JH, Lee YS, Lee HC, Kim YJ, et al. Tenofovir alafenamide for drug-resistant hepatitis B: a randomized trial for switching from tenofovir disoproxil fumarate. *Clin Gastroenterol Hepatol*. 2022;**20**(2):427-437. [PubMed ID: 33962041]. https://doi.org/10.1016/j.cgh.2021.04.045.
15. Zhang Z, Zhou Y, Yang J, Hu K, Huang Y. The effectiveness of TDF versus ETV on incidence of HCC in CHB patients: a meta analysis. *BMC Cancer*. 2019;**19**(1). 511. [PubMed ID: 31142283]. [PubMed Central ID: PMC6542001]. https://doi.org/10.1186/s12885-019-5735-9.
16. Shao J, Wang Y, Hu L, Zhang L, Lyu C. Lower risk of hepatocellular carcinoma with tenofovir than entecavir in antiviral treatment-naïve chronic hepatitis B patients: a systematic review and meta-analysis involving 90,897 participants. *Clin Exp Med*. 2023;**23**(6):2131-2140. [PubMed ID: 36648567]. https://doi.org/10.1007/s10238-023-00990-w.
17. Deng M, Tong M, Fu F, Wei D. Comparative untargeted metabolomics analysis of serum metabolic alterations in patients infected with hepatitis B virus genotypes B and C. *Arab J Chem*. 2023;**16**(10). 105155. https://doi.org/10.1016/j.arabjc.2023.105155.
18. Yang J, Lu H, Chen B, Jiang L, Zhang H, Ye P, et al. Profiling of peripheral TRBV and CD4+CD25+ Treg in CHB patients with HBeAg SC during TDF treatment. *J Immunol Res*. 2023;**1914036**:1-10. [PubMed ID: 36660247]. [PubMed Central ID: PMC9845053]. https://doi.org/10.1155/2023/1914036.
19. Papatheodoridis G, Triantos C, Hadziyannis E, Zisimopoulos K, Georgiou A, Voulgaris T, et al. Serum HBsAg kinetics and usefulness of interferon-inducible protein 10 serum in HBeAg-negative chronic hepatitis B patients treated with tenofovir disoproxil fumarate. *J Viral Hepat*. 2015;**22**(12):1079-1087. [PubMed ID: 26146764]. https://doi.org/10.1111/jvh.12434.
20. Alshehri S, Vitorino R, Saleh O, Al-Harthi S, Alahmadi A, Alotibi R, et al. Advances and applications of clinical proteomics in precision medicine. *Expert Rev Proteomics*. 2025;**22**(10):401-420. [PubMed ID: 40963397]. https://doi.org/10.1080/14789450.2025.2560919.
21. Chen Y, Wei D, Deng M. Comparative analysis of serum proteins between hepatitis B virus genotypes B and C infection by DIA-based quantitative proteomics. *Infect Drug Resist*. 2021;**14**:4701-4715. [PubMed ID: 34795487]. [PubMed Central ID: PMC8592397]. https://doi.org/10.2147/IDR.S335666.
22. Flory C, Virdi S, Schie M, Pfister S, Conze C, Thünauer R, et al. Multiomics analysis of arboviral capsid targets in mosquitoes reveals a proviral function of the chromatin-remodeling Brahma complex. *Mol Cell Proteomics*. 2026;**25**(2). 101512. [PubMed ID: 41565204]. [PubMed Central ID: PMC12927048]. https://doi.org/10.1016/j.mcpro.2026.101512.
23. Wang K, Zou Z, Wei D. Comparative liver proteomic analysis of protein expression changes in an acute-on-chronic liver failure mouse model. *Eur J Inflamm*. 2025;**23**:1-15. https://doi.org/10.1177/20587392251328475.
24. Cohen Y, Jansen T, Onwuka S, Elinav E. Advances and opportunities in measuring dietary intake: from omics to AI. *Nat Metab*. 2026;**1** - **15**(4):795-809. [PubMed ID: 41851530]. https://doi.org/10.1038/s42255-026-01494-z.
25. Huang J, Yin X, Zhang L, Yao M, Wei D, Wu Y. Serum proteomic profiling in patients with advanced Schistosoma japonicum-induced hepatic fibrosis. *Parasit Vectors*. 2021;**14**(1). 232. [PubMed ID: 33933138]. [PubMed Central ID: PMC8088642]. https://doi.org/10.1186/s13071-021-04734-1.
26. Montaigne D, Butruille L, Staels B. PPAR control of metabolism and cardiovascular functions. *Nat Rev Cardiol*. 2021;**18**(12):809-823. [PubMed ID: 34127848]. https://doi.org/10.1038/s41569-021-00569-6.

27. Ruscica M, Macchi C, Corsini A, Sirtori CR. The role of the PPAR system in diabetic cardiovascular risk and beyond. *Curr Opin Endocrinol Diabetes Obes*. 2026;**33**(1):1-7. [PubMed ID: 41263058]. https://doi.org/10.1097/MED.0000000000000943.
28. Vázquez-Carrera M, Wahli W. PPARs as key mediators in the regulation of metabolism and inflammation. *Int J Mol Sci*. 2022;**23**(9):5025. [PubMed ID: 35563416]. [PubMed Central ID: PMC9105541]. https://doi.org/10.3390/ijms23095025.
29. Duan X, Li S, Li Q, Wen W, Mezzetti O, Warner C, et al. *HBV induces liver fibrosis through the generation of reactive oxygen species in a pyruvate-dependent manner*. **1097**. 2025; 2025. [PubMed ID: 41295898]. https://doi.org/10.1097/HEP.0000000000001597.
30. Yang Y, Ge F, Luo C, Chen Y, Deng J, Yang Y, et al. Inhibition of hepatitis B virus through PPAR-JAK/STAT pathway modulation by electroacupuncture and tenofovir disoproxil fumarate combination therapy. *Int Immunopharmacol*. 2024;**143**(Pt 1). 113304. [PubMed ID: 39369463]. https://doi.org/10.1016/j.intimp.2024.113304.
31. May-Zhang L, Liu M, Black D, Tso P. Apolipoprotein A5, a unique modulator of fasting and postprandial triglycerides. *Biochim Biophys Acta Mol Cell Biol Lipids*. 2022;**1867**(9). 159185. [PubMed ID: 35644522]. https://doi.org/10.1016/j.bbalip.2022.159185.
32. Ress C, Moschen AR, Sausgruber N, Tschoner A, Graziadei I, Weiss H, et al. The role of apolipoprotein A5 in non-alcoholic fatty liver disease. *Gut*. 2011;**60**(7):985-991. [PubMed ID: 21339203]. https://doi.org/10.1136/gut.2010.222224.
33. Yang X, Deng B, Zhao W, Guo Y, Wan Y, Wu Z, et al. FABP5+lipid-loaded macrophages process tumour-derived unsaturated fatty acid signal to suppress T-cell antitumour immunity. *J Hepatol*. 2025;**82**(4):676-689. [PubMed ID: 39357545]. https://doi.org/10.1016/j.jhep.2024.09.029.
34. Zhou J, Ni W, Ling Y, Lv X, Niu D, Zeng Y, et al. Human neural stem cell secretome inhibits lipopolysaccharide-induced neuroinflammation through modulating microglia polarization by activating peroxisome proliferator-activated receptor gamma. *Stem Cells Dev*. 2022;**31**(13 - 14):369-382. [PubMed ID: 35481777]. https://doi.org/10.1089/scd.2022.0081.
35. AlAbduljader H, AlSaeed H, Alrabeea A, Sulaiman A, Haider MJA, Al-Mulla F, et al. Eicosapentaenoic acid (EPA) alleviates LPS-induced oxidative stress via the PPARα-NF-κB axis. *Oxid Med Cell Longev*. 2025;**3509596**(1). 3509596. [PubMed ID: 40530326]. [PubMed Central ID: PMC12173550]. https://doi.org/10.1155/omcl/3509596.
36. Shahtaghi NR, Soni B, Bakrey H, Bigdelitabar S, Jain SK. Beta-hydroxybutyrate: a supplemental molecule for various diseases. *Curr Drug Targets*. 2024;**25**(14):919-933. [PubMed ID: 39238395]. https://doi.org/10.2174/0113894501312168240821082224.
37. Zhou Y, Wang F, Hu M, Xia S, Li Y, Zheng S, et al. Acetoacetate ameliorates hepatic fibrosis by targeting peroxisome proliferator-activated receptor gamma to restore lipid droplets in activated hepatic stellate cells. *Pharmaceuticals (Basel)*. 2025;**18**(2):219. [PubMed ID: 40006033]. [PubMed Central ID: PMC11859973]. https://doi.org/10.3390/ph18020219.
38. Heras V, Mela V, Kompella P, Rojano E, Paz-López G, Hurtado-García L, et al. β-Hydroxybutyrate reduces body weight by modulating fatty acid oxidation and beiging in the subcutaneous adipose tissue of DIO mice. *Int J Mol Sci*. 2025;**26**(11):5064. [PubMed ID: 40507875]. [PubMed Central ID: PMC12154550]. https://doi.org/10.3390/ijms26115064.
39. Wu Y, Dahlgren C, Forsman H, Sundqvist M. LTB4 is converted into a potent human neutrophil NADPH oxidase activator via a receptor transactivation mechanism in which the BLT1 receptor activates the free fatty acid receptor 2. *Prostaglandins Leukot Essent Fatty Acids*. 2025;**205**. 102680. [PubMed ID: 40199055]. https://doi.org/10.1016/j.plefa.2025.102680.
40. Ermis E, Nargis T, Webster K, Tersey SA, Anderson RM, Mirmira RG. Leukotriene B4 receptor 2 governs macrophage migration during tissue inflammation. *J Biol Chem*. 2024;**300**(1). 105561. [PubMed ID: 38097183]. [PubMed Central ID: PMC10790086]. https://doi.org/10.1016/j.jbc.2023.105561.